JACS
JOURNAL OF THE AMERICAN CHEMICAL SOCIETY
Article
pubs.acs.org/JACS

Confining the Nucleation and Overgrowth of Rh to the {111} Facets of Pd Nanocrystal Seeds: The Roles of Capping Agent and Surface Diffusion

Shuifen Xie,[†,‡] Hsin-Chieh Peng,[§] Ning Lu,[∥] Jinguo Wang,[∥] Moon J. Kim,[∥] Zhaoxiong Xie,[‡] and Younan Xia*[,†,§,⊥]

[†]The Wallace H. Coulter Department of Biomedical Engineering, Georgia Institute of Technology and Emory University, Atlanta, Georgia 30332, United States

[‡]State Key Laboratory of Physical Chemistry of Solid Surfaces and Department of Chemistry, College of Chemistry and Chemical Engineering, Xiamen University, Xiamen 361005, China

[§]School of Chemistry and Biochemistry and [⊥]School of Chemical and Biomolecular Engineering, Georgia Institute of Technology, Atlanta, Georgia 30332, United States

[∥]Department of Materials Science and Engineering, University of Texas at Dallas, Richardson, Texas 75080, United States

Supporting Information

ABSTRACT: This article describes a systematic study of the spatially confined growth of Rh atoms on Pd nanocrystal seeds, with a focus on the blocking effect of a surface capping agent and the surface diffusion of adatoms. We initially used Pd cuboctahedrons as the seeds to illustrate the concept and to demonstrate the capabilities of our approach. Because the Pd{100} facets were selectively capped by a layer of chemisorbed Br^- or I^- ions, we were able to confine the nucleation and deposition of Rh atoms solely on the {111} facets of a Pd seed. When the synthesis was conducted at a relatively low temperature, the deposition of Rh atoms followed an island growth mode because of the high Rh−Rh interatomic binding energy. We also facilitated the surface diffusion of deposited Rh atoms by increasing the reaction temperature and decreasing the injection rate for the Rh precursor. Under these conditions, the deposition of Rh on the Pd{111} facets was switched to a layered growth mode. We further successfully extended this approach to a variety of other types of Pd polyhedral seeds that contained Pd{111} and Pd{100} facets in different proportions on the surface. As expected, a series of Pd−Rh bimetallic nanocrystals with distinctive elemental distributions were obtained. We could remove the Pd cores through selective chemical etching to generate Rh hollow nanoframes with different types and degrees of porosity. This study clearly demonstrates the importance of facet capping, surface diffusion, and reaction kinetics in controlling the morphologies of bimetallic nanocrystals during a seed-mediated process. It also provides a new direction for the rational design and synthesis of nanocrystals with spatially controlled distributions of elements for a variety of applications.

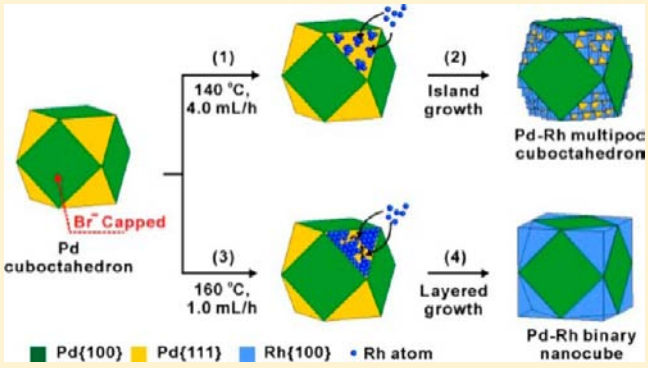

1. INTRODUCTION

Manipulating the composition, structure, and morphology of noble-metal nanocrystals is an active subject of research because it offers a powerful means to tailor their properties for a myriad of applications, including those in catalysis, plasmonics, and medicine.[1−6] In particular, bimetallic nanocrystals have received great interest owing to their plentiful variations in terms of elemental composition and spatial distribution. Compared to monometallic nanocrystals, the electronic coupling between the constituent metals of a bimetallic system can enhance their catalytic performance and optical properties or even offer novel features.[7−12] For example, both the electrochemical oxidation and reduction reactions catalyzed by Pd−Pt bimetallic nanocrystals can be markedly enhanced relative to those catalyzed by either Pd or Pt nanocrystals.[13−15] By simply varying the structure of Pd−Ag nanocrystals from dimer to core−shell and controlling the thickness of the Ag shells, one can tune the positions of their surface plasmon resonance (SPR) peaks.[16−18] Despite the progress in recent years, rational design and synthesis of bimetallic nanocrystals with novel structures and greatly enhanced properties is still a grand challenge because of

Received: August 23, 2013
Published: October 11, 2013

   dx.doi.org/10.1021/ja408768e | J. Am. Chem. Soc. 2013, 135, 16658−16667

limitations in mechanistic understanding and experimental control.

Seed-mediated growth has recently emerged as one of the most effective routes to bimetallic nanostructures.[19−21] Using this approach, the second metal is introduced into a reaction system in the form of a salt precursor, which is reduced and then deposited on the surface of preformed nanocrystals serving as the seeds for heterogeneous nucleation. For example, Pt@Pd core−shell nanocrystals with different shapes were synthesized through epitaxial deposition using preformed Pt nanocubes as the seeds.[22] Through a pH-dependent, plasmon-mediated growth process involving decahedral seeds of Au, Au−Ag bimetallic nanorods and icosahedra have also been synthesized.[23] Our group reported the overgrowth of Pt dendrites on Pd cuboctahedral seeds with greatly enhanced electrocatalytic activity toward the oxygen reduction reaction (ORR).[24,25] Owing to these previous efforts, it has been established that the nucleation and overgrowth of the second metal are governed by a number of physical parameters, such as lattice mismatch, interfacial energies, and the difference in electro-negativities/bonding energies between the two metals involved.[16,24,26,27] All of these factors need to be taken into consideration to generate bimetallic nanocrystals with desired structures. To this end, it has been demonstrated that heterogeneous nucleation and epitaxial overgrowth mode is largely determined by the correlation of surface and interfacial energies between the two metals.[28,29] For those metals with high bond dissociation and surface free energies, such as Pt and Rh, heterogeneous nucleation is greatly preferred over epitaxial layered growth.[30−35] In another respect, spatially confined overgrowth of the second metal at a selected site on the preformed seeds to generate hybrid dimeric structures is still hard to achieve. Most of the seed-mediated approaches reported in the literature typically produce conformal or dendritic core−shell bimetallic nanocrystals.

Several approaches have recently been used to overcome the aforementioned limitations. As an example, manipulating the reaction kinetics can effectively lead to asymmetric overgrowth of the second metal on the preformed seeds.[36−38] By simply tuning the reducing power of a reductant or the injection rate of a metal precursor, the nucleation and overgrowth of the second metal on a preformed seed can be spatially controlled. For example, we were able to deposit Ag or Au on any number (from one to six) of the (100) faces of a Pd cubic seed by controlling the injection rate of the precursor, generating a set of different Pd−Ag and Pd−Au hybrid nanocrystals.[17] On the other hand, the capping agent on a specific facet of the preformed seed can serve as a barrier to prevent the underlying surface from participating in nucleation and growth. For example, the deposition and overgrowth of Rh atoms on Pd cubic seeds can be confined only to the corner and edge sites to generate Pd−Rh core−frame concave nanocubes because of the blocking effect of Br^- ions chemisorbed on the Pd{100} facets.[39] Very recently, we also found that the diffusion of adatoms on the surface of a preformed seed could play an important role in determining the structure/morphology of the product of seed-mediated growth. For instance, by controlling the diffusion rate of the Pd atoms on preformed Pd cubic seeds, Pd nanocrystals with a set of morphologies, including octapods, concave cubes, cubes, and cuboctahedrons, could be obtained.[40] For all of these studies, the Pd nanocubes used as the seeds had relatively sharp corners and thus very small areas for the {111} facets. As a result, only one nucleation event could be observed on each {111} facet, making it impractical to investigate how experimental conditions will affect the possible switching from island to layer-by-layer growth.

Herein, we report a systematic study of spatially confined nucleation and deposition of Rh atoms on Pd nanocrystal seeds with different proportions of {111} and {100} facets. We used a syringe pump to control the rate at which the solution of Rh precursor was added to the reaction solution. Initially, Pd cuboctahedrons were used as the seeds to conduct the synthesis in the presence of KBr. The blocking effect of a capping agent was employed to achieve site-confined deposition of Rh atoms. When the overgrowth was operated at a relatively low temperature and a high deposition rate for the atoms, island growth was preferred for the Rh atoms deposited on the Pd{111} facets, primarily because of the high binding energy and surface free energy of Rh.[34,35,41] We carefully monitored the deposition process to demonstrate that the deposition of Rh atoms occurred solely on the Pd{111} facets. Our study indicates that the blocking effect could be exerted by both Br^- and I^- ions because of their strong binding to the Pd(100) surface. In addition, the surface diffusion of Rh atoms was facilitated to switch the deposition mode from island growth, or the Volmer−Weber (V−W) mode, to layered growth, or the Frank−van der Merwe (F−M) mode. As expected, sufficient surface diffusion of the deposited Rh atoms could reduce or even eliminate the formation of Rh islands, forming smooth Pd−Rh binary nanocubes. We also extended the Pd seeds to a number of other Pd polyhedrons to demonstrate the effect of the area of the Pd{111} facets on the spatially confined deposition and the time scale of surface diffusion for the Rh atoms. For all different types of Pd nanocrystal seeds, the site-selective deposition of Rh atoms on the Pd{111} facets could be realized by taking advantage of the blocking effect of Br^- ions chemisorbed on the Pd{100} facets. In the end, we could remove the Pd cores to generate hollow Rh nanoframes with different degrees of porosity through selective chemical etching of the Pd seeds. We note that a previous study reported the iodide-mediated island growth of Rh atoms on both Pd(100) and Pd(111) surfaces without facet selectivity.[35] Our study indicates that iodide is not an essential element for the achievement of island growth of Rh atoms on Pd nanocrystals. It is the ratio of the surface diffusion rate of adatoms to the deposition rate that controls the growth mode.

2. EXPERIMENTAL SECTION

2.1. Chemicals and Materials. Ethylene glycol (EG, lot no. K43B24) was purchased from J. T. Baker. Sodium palladium(II) tetrachloride (Na_2PdCl_4, 99.998%), sodium rhodium(III) hexachloride (Na_3RhCl_6), poly(vinyl pyrrolidone) (PVP, MW ≈ 55000), L-ascorbic acid (AA), potassium bromide (KBr), sodium bromide (NaBr), potassium iodide (KI), formaldehyde (HCHO, 37 wt % in H_2O), hydrochloric acid (HCl, 37%), and iron(III) chloride ($FeCl_3$, 97%) were all obtained from Sigma-Aldrich. All chemicals were used as received. All aqueous solutions were prepared using deionized (DI) water with a resistivity of 18.2 MΩ·cm.

2.2. Synthesis of 18-nm Pd Nanocubes. Pd nanocubes (18-nm) were synthesized by adding an aqueous Na_2PdCl_4 solution to an aqueous solution containing PVP, AA, and KBr.[42] Typically, 105 mg of PVP, 60 mg of AA, 600 mg of KBr, and 8.0 mL of DI water were mixed in a vial and preheated at 80 °C in an oil bath under magnetic stirring for 10 min. Subsequently, 57 mg of Na_2PdCl_4 was dissolved in 3.0 mL of DI water and then injected into the preheated solution with a pipet. The mixture of reagents was capped and maintained at 80 °C for 3 h. The product was collected by centrifugation, washed three

dx.doi.org/10.1021/ja408768e | J. Am. Chem. Soc. 2013, 135, 16658−16667

times with water to remove excess PVP and inorganic ions, and then redispersed in 11.0 mL of DI water.

2.3. Synthesis of Pd Polyhedral Seeds. Pd polyhedral seeds were synthesized through a seed-mediated approach according to our previous report.[43] In a typical synthesis, 8.0 mL of an aqueous solution containing 105 mg of PVP, 100 μL of HCHO, and 0.4 mL of an aqueous suspension of 18-nm Pd nanocubes was preheated at 60 °C for 5 min under magnetic stirring in a capped vial. Then, 3.0 mL of an aqueous Na_2PdCl_4 solution was injected into the preheated mixture with a pipet. The amounts of Na_2PdCl_4 for obtaining truncated cubes, cuboctahedrons, truncated octahedrons, and octahedrons were 5.7, 8.7, 17.4, and 29.0 mg, respectively. The reaction mixture was maintained at 60 °C for 3 h. The products were collected by centrifugation, washed twice with water, and then redispersed in 1.0 mL of EG.

2.4. Synthesis of Pd–Rh Bimetallic Nanocrystals. Pd–Rh bimetallic nanocrystals were prepared by slowly introducing Na_3RhCl_6 solution (in EG) into a reaction system containing Pd polyhedral seeds. In a standard procedure, 52.8 mg of AA, 54 mg of KBr, 133 mg of PVP, 1.0 mL of Pd polyhedral seeds in EG, and 12.0 mL of EG were mixed in a 50 mL three-neck flask. The mixture was preheated at 110 °C for 2 h under magnetic stirring and then ramped to the specific reaction temperature (140, 160, or 180 °C). Meanwhile, 15 mg of Na_3RhCl_6 was dissolved in 6.0 mL of EG and then added to the preheated mixture at a constant injection rate (4.0 or 1.0 mL/h). The reaction was allowed to proceed for an additional 10 min after the Na_3RhCl_6 precursor had been completely injected. The products were collected by centrifugation, washed twice with ethanol and then three times with water, and finally redispersed in 5.0 mL of DI water.

2.5. Synthesis of Rh Nanoframes. Chemical etching was conducted for the three types of Pd–Rh bimetallic nanocrystals using an acidic aqueous solution to generate Rh nanoframes. Typically, 300 mg of KBr, 50 mg of PVP, 50 mg of $FeCl_3$, 0.3 mL of HCl (37%), 5.7 mL of DI water, and 2.0 mL of an aqueous dispersion of the as-prepared Pd–Rh bimetallic nanocrystals were mixed in a 50 mL flask. Then, the mixture was heated at 100 °C in an oil bath under magnetic stirring. After 24 h, the products were collected by centrifugation, washed twice with ethanol and three times with water, and then redispersed in DI water.

2.6. Characterizations. Scanning electron microscopy (SEM) images were captured using a SU8040 cold-field-emission microscope (Hitachi) operated at 15 kV. Transmission electron microscopy (TEM) images were recorded using a JEM-1400 microscope (JEOL, Tokyo, Japan) and a Hitachi HT-7700 (Hitachi, Tokyo, Japan) operated at 120 kV. The samples were prepared by drop casting the nanocrystal dispersions on carbon-coated Cu grids and drying under ambient conditions. High-resolution TEM (HRTEM), high-angle annular dark-field scanning TEM (HAADF-STEM), and energy-dispersive X-ray (EDX) analyses were performed using a JEOL ARM200F microscope with STEM Cs corrector operated at 200 kV. X-ray photoelectron microscopy (XPS) data were collected using a Thermo K-Alpha photoelectron spectrometer with an Al Kα source.

3. RESULTS AND DISCUSSION

3.1. Site-Confined Growth of Rh on Pd Cuboctahedral Seeds. We used Pd cuboctahedrons as the seeds because each one of them is enclosed by {111} facets and {100} facets in roughly the same proportion in terms of area. This allows the influence of facet type on the nucleation and growth of Rh atoms to be evaluated easily. Figure 1 schematically illustrates how to synthetically manipulate the nucleation and growth of Rh atoms on Pd cuboctahedral seeds. In the presence of KBr, all six Pd{100} facets on the Pd cuboctahedral seed are capped by a layer of chemisorbed Br^- ions, which can serve as a barrier to prevent the deposition of Rh atoms on the Pd{100} facets. At a relatively low reaction temperature (140 °C) and high injection rate (4.0 mL/h) for the Rh precursor, the newly formed Rh atoms can nucleate and grow only on the uncovered

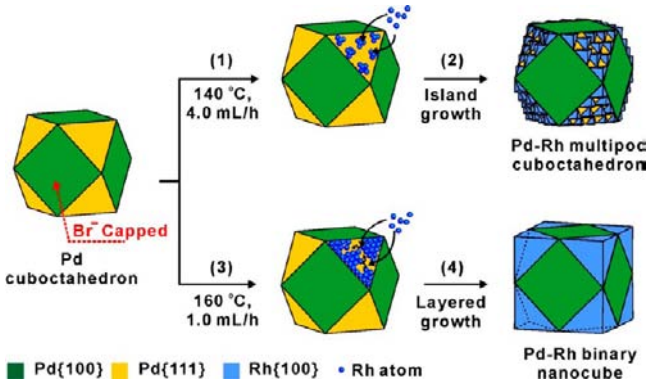

Figure 1. Schematic illustrations of the two different modes involved in the deposition of Rh on Pd cuboctahedral seeds in the presence of Br^- ions: (1) nucleation of Rh atoms at multiple sites on each Pd{111} facet, (2) continuous deposition of Rh atoms on the just-formed Rh nuclei in an island growth mode to produce a Pd–Rh multipod cuboctahedron, (3) deposition of Rh atoms on the entire area of each Pd{111} facet due to the involvement of surface diffusion, and (4) layered growth of Rh atoms on the Pd{111} facets to generate a Pd–Rh binary nanocube.

{111} facets of a Pd cuboctahedral seed. Although some portions of the Pd{111} facets are still available after the initial nucleation event, the Rh atoms formed at a later stage will be preferentially deposited on the just-formed Rh nuclei to generate multiple Rh islands on each Pd{111} facet. This island growth mode can be attributed to the strong Rh–Rh interaction due to the high interatomic binding energy and surface free energy of Rh.[34,35] The final products will be Pd–Rh bimetallic nanocrystals consisting of multiple islands of Rh anchored to the {111} facets of Pd cuboctahedral seeds.

The growth pattern of Rh atoms can be manipulated by enabling surface diffusion for the deposited Rh atoms. Surface diffusion can be enhanced by simply increasing the reaction temperature and/or extending the deposition time. When the temperature was increased to 160 °C, surface diffusion of the deposited Rh atom was greatly accelerated. At a low injection rate (1.0 mL/h) for the Rh precursor, the deposited Rh atoms had enough time to diffuse to other regions and eventually cover the entire Pd{111} surface. In this case, the formation of multiple Rh islands on each {111} facet was eliminated. As such, the overgrowth of Rh was switched from an island mode to a layered mode. Under these conditions, the Rh atoms were deposited evenly on the Pd{111} facets with full coverage. With the continuous deposition of Rh atoms, the truncated corners of the Pd cuboctahedrons were gradually filled with Rh atoms, leading to the formation of a new type of Pd–Rh binary nanocubes. Each of the cubes consisted of a Pd cuboctahedral core and eight Rh corners.

3.2. Pd–Rh Bimetallic Nanocrystals Formed under an Island Growth Mode. Figure S1 (Supporting Information) shows transmission electron microscopy (TEM) images of the as-prepared Pd cuboctahedral seeds. When observed along the ⟨100⟩ axes, a Pd cuboctahedron gives a square projection with large truncations at the four corners. We monitored the growth process by increasing the amount of Na_3RhCl_6 solution at a rate of 4.0 mL/h. The reaction system was controlled at 140 °C. Aliquots of the reaction solution (0.3 mL) were withdrawn at various time points. Figure 2 shows the morphological evolution from Pd cuboctahedrons to Pd–Rh bimetallic cuboctahedrons with multiple islands on the Pd{111} facets.

dx.doi.org/10.1021/ja408768e | J. Am. Chem. Soc. 2013, 135, 16658–16667

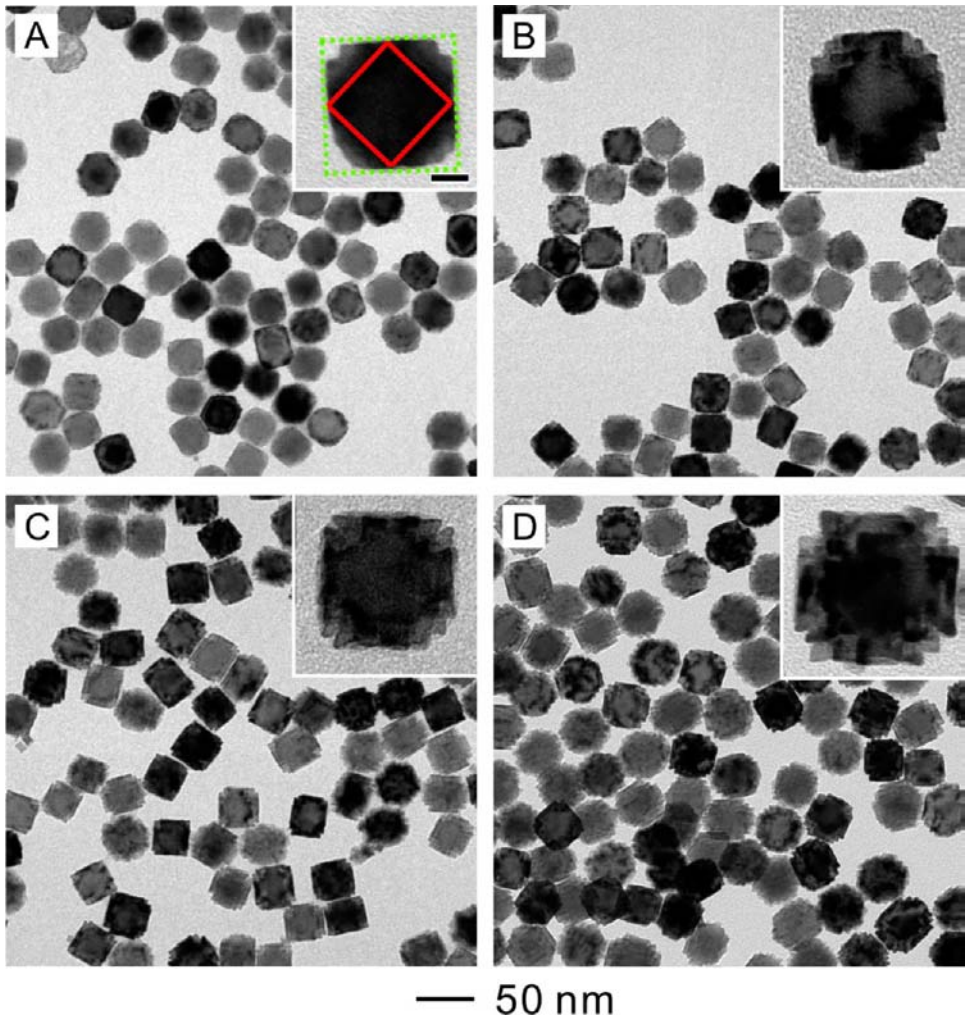

Figure 2. TEM images of Pd−Rh multipod cuboctahedrons synthesized using the standard procedure after the introduction of different volumes of Na_3RhCl_6 solution (in EG, 2.5 mg/mL): (A) 1.0, (B) 2.0, (C) 4.0, and (D) 6.0 mL. The solution was pumped into the reaction system at a rate of 4.0 mL/h. The scale bar in the first inset is 10 nm and applies to all of the insets. The red and green square boxes indicate the area of the {100} facet on the original seed and the overall profile of a Pd−Rh bimetallic nanocrystal, respectively.

When a small amount of Na_3RhCl_6 (1.0 mL, 2.5 mg/mL) was introduced into the reaction solution in the presence of KBr (Figure 2A), some salient islands appeared at the {111} facets while the {100} facets remained smooth. This observation demonstrates that the generated Rh atoms were selectively deposited as islands on the Pd{111} facets during the early stage of growth. Owing to a strong Rh−Rh interaction, those deposited Rh atoms were bound to the original deposition sites. With the increase of Na_3RhCl_6, the number of Rh islands on each {111} facet increased (Figure 2B). Subsequently, the Rh islands continuously grew to larger sizes, and finally, they evolved into multiple bumps on each of the Pd{111} facets (Figure 2C,D). During the entire growth process, the Pd{100} facets were preserved in terms of smoothness, resulting in spatially confined deposition of Rh solely on the Pd{111} facets. The low injection rate for Na_3RhCl_6 was an important factor in avoiding self-nucleation for the newly generated Rh atoms so that the Rh atoms only nucleated and grew on the Pd seeds. Figure S2 (Supporting Information) shows the products obtained at a higher injection rate (40 mL/h) for the Na_3RhCl_6 solution. Because the concentration of the Rh atoms was much higher at the beginning, most of the initially formed atoms underwent self-nucleation, and the later Rh atoms tended to grow on the small Rh seeds to generate a large number of small Rh nanocrystals. As a result, very few Rh atoms were deposited on the Pd cuboctahedral seeds.

We further characterized the structure and composition of the Pd−Rh bimetallic nanocrystals using scanning electron microscopy (SEM), high-angle annular dark-field scanning TEM (HAADF-STEM), selected-area electron diffraction (SAED), and energy-dispersive X-ray (EDX) analysis to confirm the spatially confined, island growth mode. As shown in the SEM and HAADF-STEM images (Figure 3A,B), multiple Rh islands with a triangular pyramid shape were formed on the Pd cuboctahedral seeds, giving the Pd−Rh nanocrystals a rough appearance. The inset in Figure 3A and the single Pd−Rh nanocrystal marked in Figure 3B clearly illustrate that a square region on the surface of the Pd cuboctahedral seed was kept flat, indicating the growth of Rh on Pd{100} was effectively inhibited. Figure 3C shows an HAADF-STEM image of a single Pd−Rh nanocrystal along the ⟨001⟩ zone axis, further confirming the smooth {100} facets and rough, truncated corners. Its corresponding EDX mapping analysis is shown in Figure 3D. On the square {100} facet in the center, only Pd (marked in red) was detected, whereas only Rh atoms (marked in green) were found on the truncated corners of {111} facets.

dx.doi.org/10.1021/ja408768e | J. Am. Chem. Soc. 2013, 135, 16658−16667

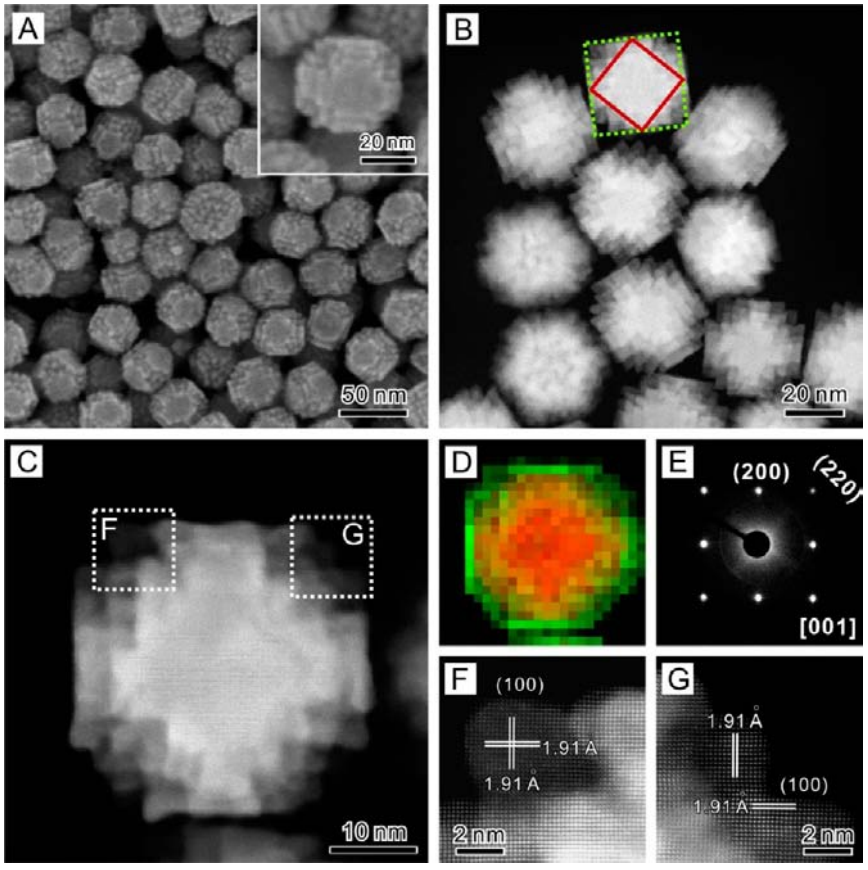

Figure 3. Characterizations of the morphology, structure, and composition of the Pd−Rh multipod cuboctahedrons prepared using the standard procedure: (A) SEM image, (B,C) HAADF-STEM images, (D) EDX mapping (green, Rh; red, Pd) of the Pd−Rh multipod cuboctahedrons in panel C, (E) SAED pattern, (F,G) atomic-resolution HAADF-STEM image of the regions marked in panel C. The red and green square boxes in panel B indicate the area of the {100} facet on the original seed and the overall profile of a Pd−Rh bimetallic nanocrystal, respectively.

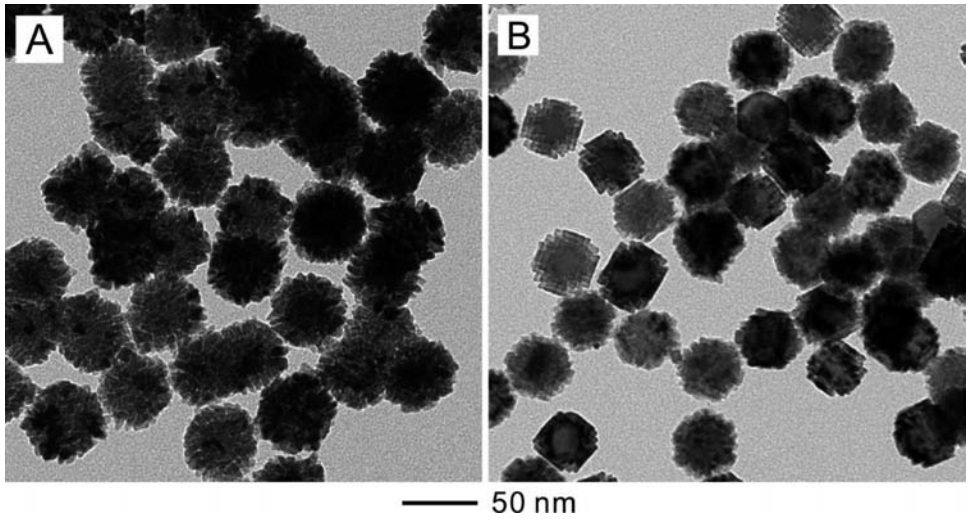

Figure 4. TEM images of Pd−Rh bimetallic nanocrystals synthesized using the standard procedure except for the following variations: (A) without the addition of KBr and (B) with an equal molar amount of NaBr substituting for the KBr.

These results further demonstrate the successful confinement of Rh atoms to the {111} facets of the Pd cuboctahedral seeds through the blocking of Pd{100} facets by chemisorbed Br^- ions. The corresponding SAED pattern in Figure 3E shows a single-crystal structure for the Pd−Rh nanocrystal, indicating that the crystal orientation of the deposited Rh was the same as that of the Pd cuboctahedral seeds. Furthermore, the atomic-resolution HAADF-STEM images on the marked corner regions of a single Pd−Rh nanocrystal (Figure 3F,G) clearly show that the main surface of the Rh portion was parallel to the Rh{200} planes (1.91 Å). This result suggests that the surfaces of the protruding Rh islands were dominated by {100} facets. Hence, each of the Rh islands can be regarded as a shrunken

dx.doi.org/10.1021/ja408768e | J. Am. Chem. Soc. 2013, 135, 16658−16667

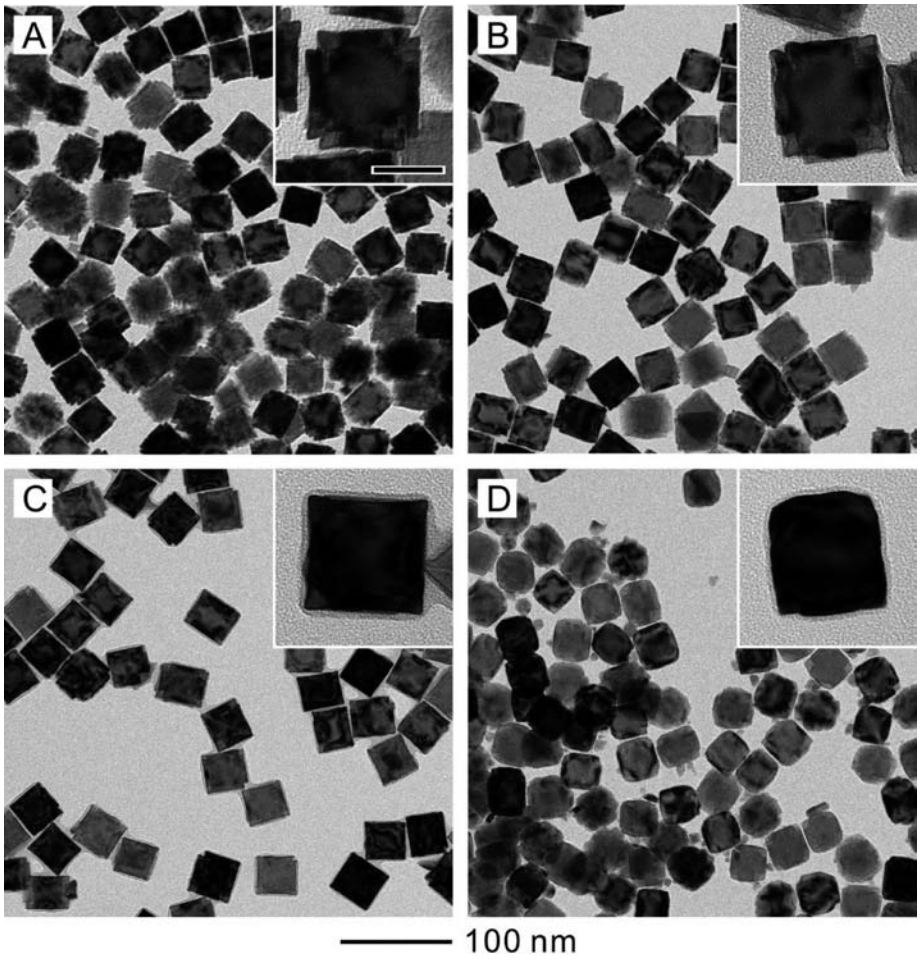

Figure 5. TEM images of Pd−Rh bimetallic nanocrystals synthesized using the standard procedure except for variations in reaction temperature and/or precursor injection rate: (A) 140 °C, 1.0 mL/h; (B) 160 °C, 4.0 mL/h; (C) 160 °C, 1.0 mL/h; and (D) 180 °C, 1.0 mL/h. The scale bar in the first inset is 20 nm and applies to all of the insets.

triangular pyramid cut from the corner of a cube and then anchored on the Pd{111} facets of the Pd cuboctahedral seeds.

3.3. Effect of Bromide Ions. As illustrated in Figure 1, the spatially confined overgrowth of Rh atoms should be attributed to the blocking effect of Br^- ions capping the Pd{100} facets. When a Pd cuboctahedral seed is immersed in a solution in the presence of Br^- ions, the six {100} facets will be capped by a layer of Br^- ions, whereas the eight {111} facets will not be capped. This argument was supported by the X-ray photoelectron spectroscopy (XPS) data. Figure S3 (Supporting Information) shows a decreasing content of surface Br^- ions with decreasing area of Pd{100} facets by comparing the as-prepared Pd nanocubes, cuboctahedrons, and octahedrons. Therefore, the deposition of Rh atoms on Pd{100} will be inhibited. The blocking effect on Pd{100} facets was observed over a broad range of concentrations for the Br^- ions. For example, the products synthesized with the addition of 5 and 100 mg of KBr showed Pd−Rh bimetallic multipods with a structure similar to what was obtained with 54 mg of KBr (Figure S4, Supporting Information). Our XPS analysis indicates that the Br^- ions adsorbed on the Pd{100} facets of the cuboctahedral seeds gradually came off during the preheating process because of the presence of reductive conditions (Figure S5A, Supporting Information).[44] Although the Br^- ions coming off the cuboctahedrons were still present in the reaction solution, their concentration was too low to exert any capping effect during the seeded growth process. We also conducted a synthesis without the addition of KBr. As shown by both the TEM and SEM images (Figure 4A and Figure S6, Supporting Information), the Pd cuboctahedral seeds were completely covered by a dense, polycrystalline shell of Rh after the overgrowth in the absence of Br^- ions, indicating isotropic deposition and an island growth mode. In addition, when KBr was substituted by an equimolar amount of NaBr, similar spatially confined Pd−Rh bimetallic nanocrystals could also be obtained (Figure 4B). These results clearly confirmed the blocking effect of Br^- ions for the Pd{100} facets during the aforementioned spatially confined overgrowth of Rh on Pd cuboctahedral seeds. Moreover, it is notable that the Rh islands on the Pd seeds obtained in the absence of KBr were irregular in shape (Figure 4A and Figure S6, Supporting Information), whereas those obtained in the presence of KBr were encased by Rh{100} facets with a triangular pyramid shape. The expression of Rh{100} facets on the Rh islands in the spatially confined Pd−Rh cuboctahedrons (Figure 3F,G) could also be attributed to the presence of Br^- ions because Br^- ions can also promote the formation of Rh(100) surface through chemisorption.[45−47] Overall, Br^- ions played two key roles in this spatially confined synthesis of Pd−Rh bimetallic nanocrystals: (i) capping the Pd{100} facets of the Pd cuboctahedral seeds and thus blocking the deposition of Rh

dx.doi.org/10.1021/ja408768e | J. Am. Chem. Soc. 2013, 135, 16658−16667

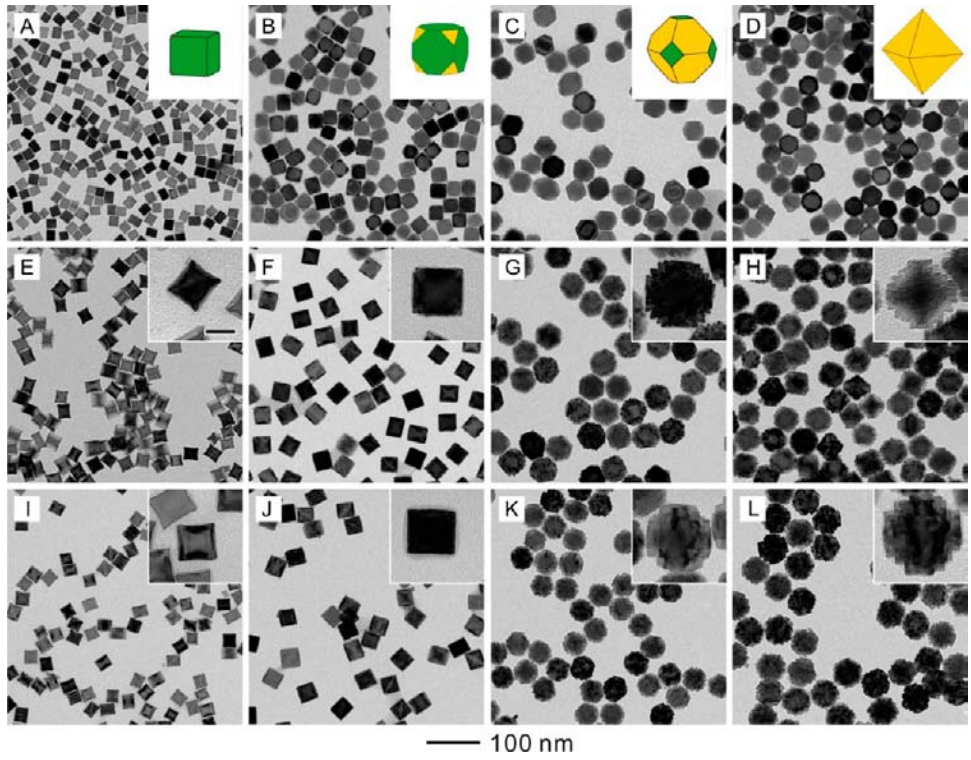

Figure 6. (A–D) TEM images of Pd nanocubes, truncated nanocubes, truncated octahedrons, and octahedrons that were employed as the seeds for the overgrowth of Rh. (E–H) TEM images of the resultant Pd–Rh bimetallic nanocrystals synthesized at 140 °C with an injection rate of 4.0 mL/h for the precursor. (I–L) TEM images of the resultant Pd–Rh bimetallic nanocrystals that were synthesized at 160 °C with an injection rate of 1.0 mL/h for the precursor. The scale bar in the inset of panel E is 20 nm and applies to all of the insets.

atoms on these facets and (ii) capping the newly generated Rh surface and thus promoting the formation of Rh{100} facets.

The blocking effect on the Pd{100} facets may also be exerted by other halide ions such as Cl^- and I^-. As the interactions between halide ions and noble metals generally increase in the order $Cl^- < Br^- < I^-$,[48,49] it is expected that the capping strength of Cl^- on Pd(100) surface will be too weak to block the deposition of Rh on the Pd{100} facets. For example, the reaction solution without the addition of KBr also contained many Cl^- ions that were released from the Na_3RhCl_6 precursor, but no blocking effect was observed (Figure 4A and Figure S6, Supporting Information). On the other hand, I^- ions exhibit strong binding toward the Pd(100) surface (Figure S5B, Supporting Information).[50] Hence, when the synthesis was conducted using an equimolar amount of KI to substitute KBr in the standard procedure, the Pd{100} facets could also be blocked by I^- ions (Figure S7, Supporting Information).

3.4. Involvement of Surface Diffusion in the Synthesis of Pd–Rh Binary Nanocubes. On the surface of a solid material, surface diffusion is a general process that is responsible for the motion of adatoms, molecules, and clusters.[51,52] In an overgrowth process, the growth pattern is largely determined by the ratio between the rates of atom deposition and surface diffusion.[40] Therefore, the final morphology of a nanocrystal can be well controlled by finely adjusting the participation of surface diffusion during an overgrowth process. For island growth, the deposited metal atoms were fixed at the deposition sites. Therefore, the rate of surface diffusion was much lower than that of deposition. When the diffusion rate of the deposited Rh atoms was increased, the Rh atoms would be more evenly deposited on the Pd{111} facets. To enhance the influence of surface diffusion, one can decrease the deposition rate and/or increase the rate of surface diffusion. In our synthesis, the deposition rate of Rh atoms can be readily controlled by simply adjusting the injection rate of the Rh precursor. A lower deposition rate of Rh atoms could provide more time for the adatoms to diffuse to a more stable site. Figure 5A shows TEM images of Pd–Rh bimetallic nanocrystals obtained by decreasing the precursor injection rate from 4.0 to 1.0 mL/h. Although the Rh islands were not completely eliminated, the number of Rh islands on each Pd{111} facet was greatly reduced, and the size of each Rh island was increased, indicating the promotion of surface diffusion.

In another respect, surface diffusion is typically a thermally promoted process. Therefore, the diffusion rate of the deposited Rh atoms can be accelerated by increasing the reaction temperature. When the reaction temperature was raised to 160 °C and the precursor injection rate was maintained at 4 mL/h, the as-obtained Pd–Rh bimetallic nanocrystals were shaped into a cubic prototype with a few bifurcates at the corners (Figure 5B) because of the enhanced diffusion of Rh atoms. To achieve a sufficient surface diffusion, we further synthesized Pd–Rh bimetallic nanocrystals by simultaneously increasing the reaction temperature to 160 °C and decreasing the precursor injection rate to 1.0 mL/h. Under these conditions, the bifurcates at the corners of the obtained Pd–Rh bimetallic nanocrystal were completely eliminated, and integrated Pd–Rh binary nanocubes were formed (Figure 5C). Each of the Pd–Rh binary nanocubes can be regarded as a combination of a Pd cuboctahedral core and eight Rh triangular pyramid corners. When the reaction temperature was too high, the corners of the Pd–Rh binary nanocubes became blunt or truncated (Figure 5D), primarily due to the excessive atomic diffusion from the corners to the side faces. As such, by

dx.doi.org/10.1021/ja408768e | J. Am. Chem. Soc. 2013, 135, 16658–16667

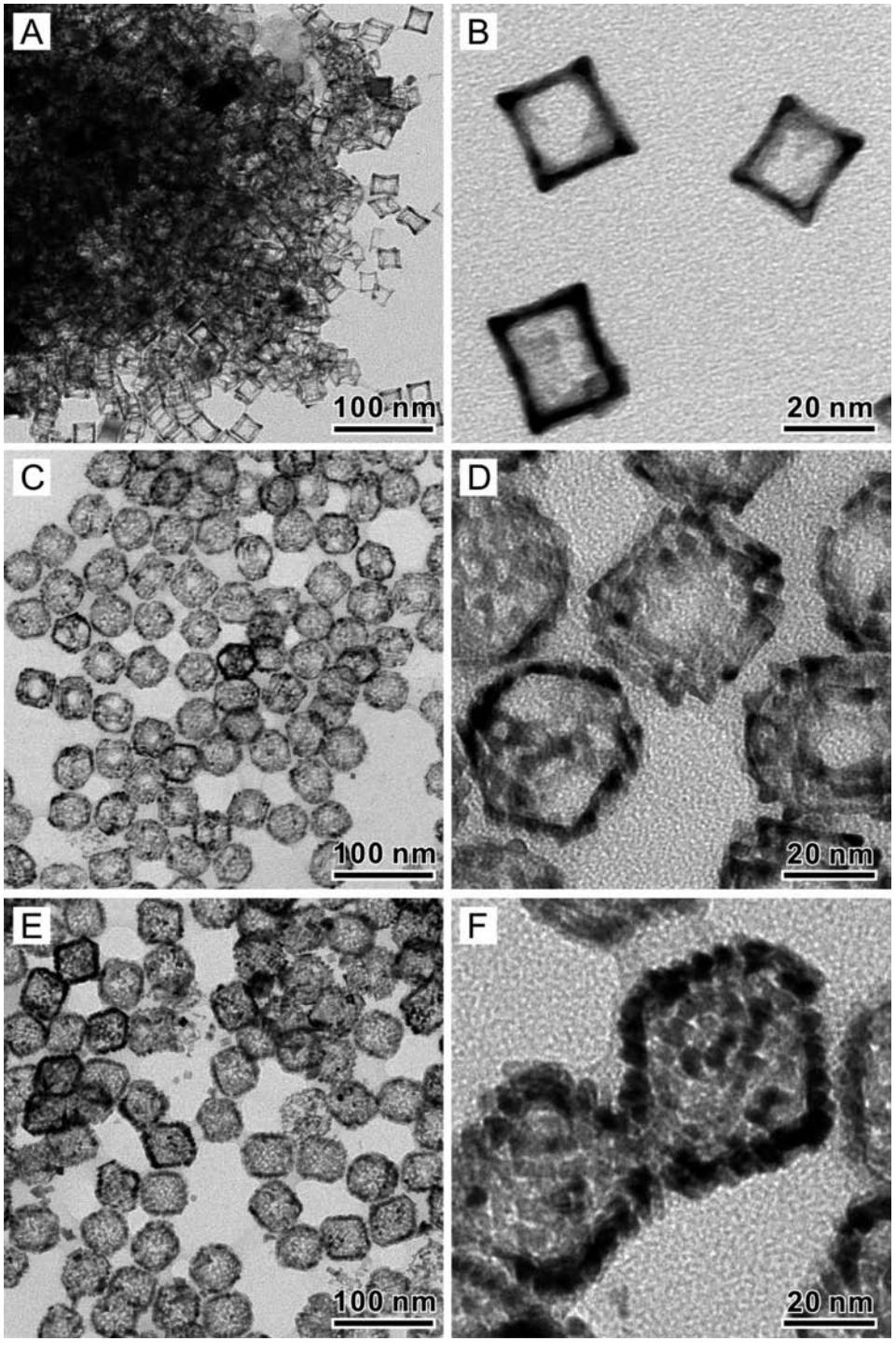

Figure 7. Rh nanoframes prepared by selectively etching away the Pd cores. (A,B) TEM images of Rh cubic nanoframes prepared from the Pd−Rh core−frame concave nanocubes shown in Figure 6E. (C,D) TEM images of Rh cuboctahedral nanoframes derived from the Pd−Rh multipod cuboctahedrons shown in Figure 2D. (E,F) TEM images of Rh octahedral nanoframes prepared from the Pd−Rh multipod octahedrons shown in Figure 6H.

adjusting the surface diffusion during the overgrowth process, the growth of Rh atoms could be successfully switched from island mode to layered mode, and the structures of the obtained Pd−Rh bimetallic nanocrystals were converted from multipod cuboctahedrons to binary nanocubes.

3.5. Influence of the Area of Pd{111} Facets. During the overgrowth process, the area of each Pd{111} facet can influence the nucleation and surface diffusion of Rh atoms. To examine the effect of the Pd{111} area, we extended the synthesis of Pd−Rh bimetallic nanocrystals from Pd cuboctahedral seeds to a number of other Pd polyhedral seeds, including cubes, truncated cubes, truncated octahedrons, and octahedrons. The morphologies of these Pd polyhedral seeds are shown in Figure 6A−D. Compared to the area of Pd cuboctahedrons, the area of Pd{111} on Pd truncated nanocubes and nanocubes is reduced, whereas this area is increased on Pd truncated octahedrons and octahedrons. Figure 6E−H shows TEM images of the resultant Pd−Rh bimetallic

dx.doi.org/10.1021/ja408768e | J. Am. Chem. Soc. 2013, 135, 16658−16667

nanocrystals synthesized under conditions with slow atomic surface diffusion (140 °C, 4 mL/h). When Pd nanocubes were used as the seeds, the tiny truncated corners could serve as the sites for the deposition of Rh with only a single nucleation event on each small {111} facet. Some of the deposited Rh atoms could diffuse from the corner sites to the edge sites, generating Pd−Rh core−frame concave nanocubes. When the area of Pd{111} was enlarged by changing from cubes to truncated cubes, truncated octahedrons, and octahedrons, the number of Rh islands on each Pd{111} facet increased. As shown by both the TEM and SEM images (Figure 6H and Figure S8, Supporting Information), after the overgrowth, the Pd octahedral seeds were completely covered by a dense array of Rh triangular pyramids. Figure 6I−L shows TEM images of the resultant Pd−Rh bimetallic nanocrystals synthesized under conditions with enhanced surface atomic diffusion (160 °C, 1 mL/h). For the cubic seeds, it is obvious that some of the Rh atoms diffused from the corners to the side faces, generating Pd−Rh core−shell concave nanocubes (Figure 6I). The side face could be further tuned from concave to flat by increasing the reaction temperature to 180 °C (Figure S9, Supporting Information). For the Pd truncated cubes, the bifurcates at the corners were eliminated, to produce Pd−Rh binary nanocubes (Figure 6J). However, for both Pd truncated octahedrons and octahedrons, the surface diffusion could only reduce the number of Rh islands on each Pd{111} facet and increase their sizes (Figure 6K,L). In this case, the large area of Pd{111} facets greatly increased the distance that the Rh atoms could diffuse across, which prevented complete integration of the Rh islands.

3.6. Rh Nanoframes from Pd−Rh Bimetallic Nanocrystals through Selective Etching. One of the advantages of the spatially confined growth of bimetallic nanocrystals is the difference in reactivity between the two metal components. As we demonstrated in a previous work, the Pd cubic core can be selectively removed from the Pd−Rh core−frame concave nanocrystal to generate a cubic nanoframe consisting of pure Rh because Rh exhibits a much higher oxidative corrosion resistance than Pd.[39,53] This selective etching was conducted in an aqueous solution containing the Fe^{III}/Br^{-} pair, based on the reaction[39]

$$Pd + 2Fe^{3+} + 4Br^{-} \xrightarrow{\Delta} PdBr_4^{2-} + 2Fe^{2+}$$

The final structure of the Rh nanoframes was apparently determined by the structure of the Pd−Rh bimetallic nanocrystals. To further systematically control the structure of the Rh nanoframes, we chose three typical Pd−Rh bimetallic nanocrystals including Pd−Rh core−frame nanocubes (Figure 6E), Pd−Rh multipod cuboctahedrons (Figure 2D), and Pd−Rh multipod octahedrons (Figure 6H), to conduct the selective etching of Pd cores. Figure 7 shows TEM images of the three resultant Rh nanoframes with different degrees of porosity. As the entire {100} surfaces of the Pd cores were exposed in the Pd−Rh core−frame nanocubes, the Rh cubic frames resulted in a cubic, skeleton-like frame structure with the greatest opening after the removal of the Pd cubic cores (Figure 7A,B). After the removal of the Pd cores from the Pd−Rh multipod cuboctahedrons, large caves emerged in the region of the bare Pd{100} facets. Novel Rh cuboctahedral nanoframes made of polycrystalline Rh triangular pyramids were obtained (Figure 7C,D). Analogously, Rh octahedral nanoframes were obtained by the removal of the Pd cores away from the Pd−Rh multipod octahedrons. The Rh octahedral nanoframes, with all of the frame walls consisting of a dense array of polycrystalline Rh triangular pyramids, took an integral octahedral nanocage structure without apparent caves on the surface (Figure 7E,F). Hence, the morphologies and degrees of porosity for the Rh nanoframes could easily be controlled by using different types of Pd polyhedral seeds in the aforementioned spatially confined synthesis. We believe that these Rh nanoframe structures are of great value in catalytic applications owing to their large surface areas and unique hollow/open structures.

4. CONCLUSIONS

In summary, we have systematically investigated the spatially confined growth of Rh on Pd nanocrystal seeds that involved the blocking effect of a surface capping agent and the variation of the surface diffusion rate for the adatoms. Mechanistic understanding was achieved by using well-defined Pd cuboctahedrons as the seeds. Because the Pd{100} facets were selectively capped by a layer of chemisorbed Br^{-} or I^{-} ions, we were able to confine the nucleation and deposition of Rh atoms solely to the {111} facets of a Pd seed. When the synthesis was conducted at a relatively low temperature to decelerate surface diffusion, the deposition of Rh atoms followed an island mode due to the high bond dissociation energy and surface free energy of Rh. This site-selected deposition and island nucleation/growth were clearly revealed by monitoring the morphological evolution and structural analysis of the final Pd−Rh multipod cuboctahedrons. Significantly, the diffusion of the deposited Rh atoms could be accelerated during the deposition process by increasing the reaction temperature. When the injection rate for the precursor was reduced, the growth was switched from an island to a layered mode. We also extended this new strategy to a number of other types of Pd polyhedral seeds consisting of Pd{111} and Pd{100} facets in different proportions to investigate the effect of the Pd{111} area on the surface diffusion process. To this end, a variety of Pd−Rh bimetallic nanocrystals with distinctive elemental distributions were obtained. By taking advantage of the well-defined spatial distributions of elements for the Pd−Rh nanocrystals, we could remove the Pd cores to generate Rh nanoframes with different types and degrees of porosity through selective chemical etching. We believe that both the novel Pd−Rh nanocrystals and the Rh nanoframes are of great interest for a variety of applications, especially in catalysis.

■ ASSOCIATED CONTENT

Supporting Information

TEM images of the as-prepared Pd cuboctahedral seeds; TEM images of the products synthesized with variations in reaction conditions; XPS data of the Br 3d on the surface of the as-prepared Pd nanocubes, Pd cuboctahedrons, and octahedrons; SEM images of the Pd−Rh bimetallic nanocrystals with Pd cuboctahedrons as the seeds without the addition of KBr; XPS data for Br 3d and I 3d on the surface of the Pd cuboctahedrons before and after the preheating process; SEM images of the Pd−Rh multipod octahedrons; and TEM images of the Pd−Rh core−shell nanocubes. This material is available free of charge via the Internet at http://pubs.acs.org.

■ AUTHOR INFORMATION

Corresponding Author

E-mail: younan.xia@bme.gatech.edu

Notes

The authors declare no competing financial interest.

■ ACKNOWLEDGMENTS

This work was supported in part by a grant from the NSF (DMR-1215034), a DOE subcontract from the University of Wisconsin at Madion (DE-FG02-05ER15731), and start-up funds from Georgia Institute of Technology. As a visiting Ph.D. student from Xiamen University, S.X. was also partially supported by the China Scholarship Council (CSC).

■ REFERENCES

(1) Burda, C.; Chen, X.; Narayanan, R.; El-Sayed, M. A. *Chem. Rev.* **2005**, *105*, 1025−1102.
(2) Xia, Y.; Xiong, Y.; Lim, B.; Skrabalak, S. E. *Angew. Chem., Int. Ed.* **2009**, *48*, 60−103.
(3) An, K.; Somorjai, G. A. *ChemCatChem* **2012**, *4*, 1512−1524.
(4) Tian, N.; Zhou, Z.-Y.; Sun, S.-G.; Ding, Y.; Wang, Z. L. *Science* **2007**, *316*, 732−735.
(5) Rosi, N. L.; Mirkin, C. A. *Chem. Rev.* **2005**, *105*, 1547−1562.
(6) Dreaden, E. C.; Mackey, M. A.; Huang, X.; Kang, B.; El-Sayed, M. A. *Chem. Soc. Rev.* **2011**, *40*, 3391−3404.
(7) Cozzoli, P. D.; Pellegrino, T.; Manna, L. *Chem. Soc. Rev.* **2006**, *35*, 1195−1208.
(8) Tao, F.; Grass, M. E.; Zhang, Y.; Butcher, D. R.; Renzas, J. R.; Liu, Z.; Chung, J. Y.; Mun, B. S.; Salmeron, M.; Somorjai, G. A. *Science* **2008**, *322*, 932−934.
(9) Stamenkovic, V. R.; Mun, B. S.; Arenz, M.; Mayrhofer, K. J. J.; Lucas, C. A.; Wang, G.; Ross, P. N.; Markovic, N. M. *Nat. Mater.* **2007**, *6*, 241−247.
(10) Mazumder, V.; Chi, M.; More, K. L.; Sun, S. *Angew. Chem., Int. Ed.* **2010**, *49*, 9368−9372.
(11) Gu, J.; Zhang, Y.-W.; Tao, F. *Chem. Soc. Rev.* **2012**, *41*, 8050−8065.
(12) Wu, J.; Li, P.; Pan, Y.-T.; Warren, S.; Yin, X.; Yang, H. *Chem. Soc. Rev.* **2012**, *41*, 8066−8074.
(13) Wang, J. X.; Inada, H.; Wu, L.; Zhu, Y.; Choi, Y.; Liu, P.; Zhou, W.-P.; Adzic, R. R. *J. Am. Chem. Soc.* **2009**, *131*, 17298−17302.
(14) Yin, A.-X.; Min, X.-Q.; Zhang, Y.-W; Yan, C.-H. *J. Am. Chem. Soc.* **2011**, *133*, 3816−3819.
(15) Zhang, H.; Jin, M.; Xia, Y. *Chem. Soc. Rev.* **2012**, *41*, 8035−8049.
(16) Zeng, J.; Zhu, C.; Tao, J.; Jin, M.; Zhang, H.; Li, Z.-Y.; Zhu, Y.; Xia, Y. *Angew. Chem., Int. Ed.* **2012**, *51*, 2354−2358.
(17) Zhu, C.; Zeng, J.; Tao, J.; Johnson, M. C.; Schmidt-Krey, I.; Blubaugh, L.; Zhu, Y.; Gu, Z.; Xia, Y. *J. Am. Chem. Soc.* **2012**, *134*, 15822−15831.
(18) Gong, J.; Zhou, F.; Li, Z.; Tang, Z. *Chem. Commun.* **2013**, *49*, 4379−4381.
(19) Yu, H.; Gibbons, P. C.; Kelton, K. F.; Buhro, W. E. *J. Am. Chem. Soc.* **2001**, *123*, 9198−9199.
(20) Skrabalak, S. E.; Xia, Y. *ACS Nano* **2009**, *3*, 10−15.
(21) Wang, D.; Li, Y. *Adv. Mater.* **2011**, *23*, 1044−1060.
(22) Habas, S. E.; Lee, H.; Radmilovic, V.; Somorjai, G. A.; Yang, P. *Nat. Mater.* **2007**, *6*, 692−697.
(23) Langille, M. R.; Zhang, J.; Mirkin, C. A. *Angew. Chem., Int. Ed.* **2011**, *50*, 3543−3547.
(24) Lim, B.; Jiang, M.; Camargo, P. H. C.; Cho, E. C.; Tao, J.; Lu, X.; Zhu, Y.; Xia, Y. *Science* **2009**, *324*, 1302−1305.
(25) Lim, B.; Jiang, M.; Yu, T.; Camargo, P. H. C.; Xia, Y. *Nano Res.* **2010**, *3*, 69−80.
(26) Fan, F.-R.; Liu, D.-Y.; Wu, Y.-F; Duan, S.; Xie, Z.-X.; Jiang, Z.-Y.; Tian, Z.-Q. *J. Am. Chem. Soc.* **2008**, *130*, 6949−6951.
(27) Peng, Z.; Yang, H. *Nano Today* **2009**, *4*, 143−164.
(28) Bauer, E.; van der Merwe, J. H. *Phys. Rev. B* **1986**, *33*, 3657−3671.
(29) Jiang, M.; Lim, B.; Tao, J.; Camargo, P. H. C.; Ma, C.; Zhu, Y.; Xia, Y. *Nanoscale* **2010**, *2*, 2406−2411.
(30) Zhou, S.; Mcllwrath, K.; Jackson, G.; Eichhorn, B. *J. Am. Chem. Soc.* **2006**, *128*, 1780−1781.
(31) Kim, Y.; Hong, J. W.; Lee, Y. W.; Kim, M.; Kim, D.; Yun, W. S.; Han, S. W. *Angew. Chem., Int. Ed.* **2010**, *49*, 10197−10201.
(32) Wang, L.; Yamauchi, Y. *J. Am. Chem. Soc.* **2010**, *132*, 13636−13638.
(33) Kobayashi, H.; Lim, B.; Wang, J.; Camargo, P. H. C.; Yu, T.; Kim, M. J.; Xia, Y. *Chem. Phys. Lett.* **2010**, *494*, 249−254.
(34) Chantry, R. L.; Siriwatcharapiboon, W.; Horswell, S. L.; Logsdail, A. J.; Johnston, R. L.; Li, Z. Y. *J. Phys. Chem. C* **2012**, *116*, 10312−10317.
(35) Sneed, B. T.; Kuo, C.-H.; Brodsky, C. N.; Tsung, C.-K. *J. Am. Chem. Soc.* **2012**, *134*, 18417−18426.
(36) Lee, H.; Habas, S. E.; Somorjai, G. A.; Yang, P. *J. Am. Chem. Soc.* **2008**, *130*, 5406−5407.
(37) Lim, B.; Kobayashi, H.; Yu, T.; Wang, J.; Kim, M. J.; Li, Z.-Y.; Rycenga, M.; Xia, Y. *J. Am. Chem. Soc.* **2010**, *132*, 2506−2507.
(38) He, G.; Zeng, J.; Jin, M.; Zhang, H.; Lu, N.; Wang, J.; Kim, M. J.; Xia, Y. *ChemCatChem* **2012**, *4*, 1668−1674.
(39) Xie, S.; Lu, N.; Xie, Z. X.; Wang, J.; Kim, M. J.; Xia, Y. *Angew. Chem., Int. Ed.* **2012**, *51*, 10266−10270.
(40) Xia, X.; Xie, S.; Liu, M.; Peng, H.-C.; Lu, N.; Wang, J.; Kim, M. J.; Xia, Y. *Proc. Natl. Acad. Sci. U.S.A.* **2013**, *110*, 6669−6673.
(41) Vitos, L.; Ruban, A. V.; Skriver, H. L.; Kollár, J. *Surf. Sci.* **1998**, *411*, 186−202.
(42) Jin, M.; Liu, H.; Zhang, H.; Xie, Z. X.; Liu, J.; Xia, Y. *Nano Res.* **2011**, *4*, 83−91.
(43) Jin, M.; Zhang, H.; Xie, Z. X.; Xia, Y. *Energy Environ. Sci.* **2012**, *5*, 6352−6357.
(44) Peng, H.-C.; Xie, S.; Park, J.; Xia, X.; Xia, Y. *J. Am. Chem. Soc.* **2013**, *135*, 3780−3783.
(45) Zhang, Y.; Grass, M. E.; Kuhn, J. N.; Tao, F.; Habas, S. E.; Huang, W.; Yang, P.; Somorjai, G. A. *J. Am. Chem. Soc.* **2008**, *130*, 5868−5869.
(46) Zhang, Y.; Grass, M. E.; Huang, W.; Somorjai, G. A. *Langmuir* **2010**, *26*, 16463−16468.
(47) Zhang, H.; Li, W.; Jin, M.; Zeng, J.; Yu, T.; Yang, D.; Xia, Y. *Nano Lett.* **2011**, *11*, 898−903.
(48) Carrasquillo, A.; Jeng, J.-J., Jr.; Barriga, R. J.; Temesghen, W. F.; Soriaga, M. P. *Inorg. Chim. Acta* **1997**, *255*, 249−254.
(49) Xiong, Y.; Cai, H.; Wiley, B. J.; Wang, J.; Kim, M. J.; Xia, Y. *J. Am. Chem. Soc.* **2007**, *129*, 3665−3675.
(50) Huang, X.; Z.; Zheng, N. *J. Am. Chem. Soc.* **2009**, *131*, 4602−4603.
(51) Oura, K.; Lifshits, V. G.; Saranin, A. A.; Zotov, A. V.; Katayama, M. *Surface Science: An Introduction*, 1st ed.; Springer-Verlag: Berlin, 2003.
(52) Antczak, G.; Ehrlich, G. *Surf. Sci. Rep.* **2007**, *62*, 39−61.
(53) Llopis, J.; Vázquez, M. *Electrochim. Acta* **1964**, *9*, 1655−1663.